Application Note



June, 2025

Keywords or phrases:

Single-use mixer, Flexsafe® Pro Mixer, powder dissolution, CFD, computational fluid dynamics, process validation, mixing

Computational Fluid Dynamics for Enhancing Dissolution Applications in Biopharmaceutical Manufacturing

Behnam Partopour¹, Abhinav Hazarika², Johannes Wutz³, John Thomas⁴ and David Menahem⁵

- ¹ Sartorius Stedim North America, Corporate Research, Marlborough MA 01752, USA
- $^{\rm 2}$ Sartorius Stedim Biotech GmbH, August-Spindler-Str. 11 \cdot 37079 Göttingen
- ³ MStar-CFD, M-Star Center Europe GmbH, Sargstedt, Germany
- 4 M-Star Simulations, LLC, 225 Franklin St, Floor 26, Boston, MA 02110, USA
- ⁵ Sartorius Stedim FMT S.A.S, 13400 Aubagne, France

Correspondence

*Email: david.menahem@sartorius.com

Abstract

Efficient dissolution operations, such as the preparation of buffers and media, are a critical aspect of biopharmaceutical manufacturing, influencing both product quality and productivity. In this study, we explore the application of computational fluid dynamics (CFD) to optimize dissolution processes – specifically buffer preparation – in large-scale biomanufacturing. Using MStar-CFD software, we model the hydrodynamics and dissolution dynamics in single-use mixing systems, such as Flexsafe® Bags and Flexsafe® Pro Mixer systems, to enhance buffer formulation. Experimental results demonstrate the system's high efficiency, with rapid dissolution and consistent mixing times across varying volumes (50 L, 200 L, and 1,000 L).

We compared CFD simulations with experimental data, finding good agreement and confirming the model's ability to accurately predict dissolution dynamics without relying on fitting parameters. The integration of CFD into buffer preparation workflows offers significant advantages in process optimization, scalability, and risk reduction, supporting the ongoing advancement of biopharmaceutical manufacturing technologies. This study provides valuable insights into the use of CFD for improving operational efficiency, reducing costs, and achieving reproducible outcomes in biomanufacturing environments.

Introduction

Buffer and media preparation play a pivotal role in the production of biopharmaceuticals, serving as foundational components in upstream and downstream processes. These solutions provide the essential environment to maintain the process's stability, pH, and solubility. The precision and reliability of buffer and media formulation directly influence the efficiency of monoclonal antibody (mAb) production and product quality. Any deviations or inconsistencies in the preparation process can compromise product viability, reduce yield, and adversely affect the overall bioprocessing workflow, underscoring the need for meticulous optimization strategies.

As biopharmaceutical manufacturing transitions towards intensified and continuous processes, the demand for robust and scalable buffer and media preparation systems becomes even greater. Advancements in technology, such as automated buffer dilution systems and improved media formulation strategies, have significantly enhanced productivity while reducing operational costs, facility footprint, and human error.²

For example, optimizing buffer and media workflows has been shown to streamline production and enable flexible manufacturing, addressing the growing need for rapid scalability in response to market demands.³ Moreover, minimizing buffer preparation times and storage requirements aligns with the industry's sustainability goals, reducing resource consumption and waste.⁴ Recent studies and best practices show how these approaches are being integrated into modern biopharmaceutical facilities, emphasizing their importance in maintaining high-quality standards and achieving efficient therapeutic production.

Computational fluid dynamics (CFD) has become an essential tool for the design, optimization, and control of fluid management systems in the biopharmaceutical industry⁵ Advanced CFD simulations can provide spatiotemporal-resolved information regarding hydrodynamics and transport phenomena in bioreactors, mixing tanks, and other fluid management equipment and consumables.⁶ These simulations can significantly reduce the costs and risks associated with biomanufacturing and increase the speed toward large-scale commercial manufacturing.

In this study, we evaluate the application of such CFD simulations, using MStar-CFD software, for in silico assessment of dissolution processes, which can directly be applied to reduce costs and risks while increasing the speed of media and buffer preparation in biomanufacturing.

Experimental Method

Materials and Equipment

The study used Flexsafe® Pro Mixer Bags and Flexsafe® Pro Mixer single-use systems, available in 50 L, 200 L, and 1,000 L sizes. These bags are designed to maintain a sterile and flexible environment for buffer preparation, ensuring the solution's integrity throughout the process. Powder transfer bags of 15 L and 30 L capacities were used to facilitate the addition of powders, minimizing contamination risk and ensuring accurate material transfer. The chemicals used for buffer preparation included Tris base, Tris HCl, citric acid, and sodium citrate, all of which are commonly employed in biomanufacturing due to their buffering capacity and stability.⁷ Deionized water was used as the solvent to ensure the final solutions were free from impurities that could affect buffer performance. The equipment setup included a Palletank® for Mixing, integrated with a powder bag holder to support the powder transfer process. The Palletank® provides a stable and controlled mixing environment, ensuring even powder distribution throughout the solution. The Flexsafe® Pro Mixer drive unit facilitated the mixing operations, providing the necessary mechanical agitation to dissolve the powders and achieve a homogeneous solution. The setup is shown in Figure 1.

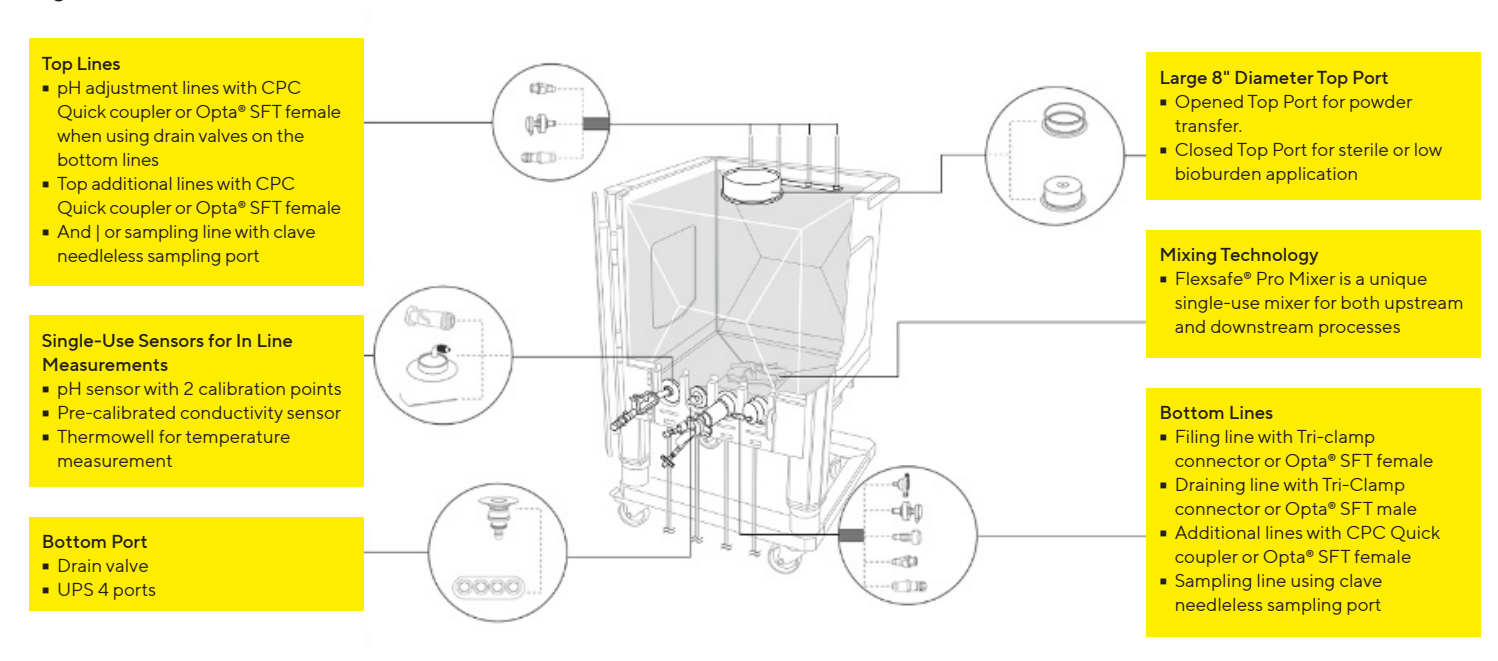
Preparation of Solutions

The Flexsafe® Pro Mixer Bags were initially filled with deionized water to 80% of the target volume, which varied between 50 L, 200 L, and 1,000 L depending on the specific experiment. This initial filling step is crucial to ensure sufficient liquid to facilitate the dissolution of the powders. The impeller speed was adjusted according to the nominal test volume to prevent foaming or splashing, which could lead to material loss and affect the final concentration of the solution. Specifically, the impeller speed was set at 300 rpm for 50 L, 500 rpm for 200 L, and 750 rpm for 1,000 L. These speeds were chosen based on previous studies and manufacturer recommendations to ensure optimal mixing without damaging the Flexsafe® Pro Mixer Bags.8

Addition of Powders

The powders were introduced into the Flexsafe® Pro Mixer Bags using 15 L or 30 L powder transfer bags. This step was carefully controlled to ensure the powders were added slowly and evenly, preventing clumping and ensuring complete dissolution. Tris Base and Tris HCl were added sequentially to prepare Tris buffer. Tris base is a weak base that provides buffering capacity, while Tris HCl is the hydrochloride salt of

Figure 1: Schematics of the Flexsafe® Pro Mixer



Tris, which helps adjust the solution's pH. For the preparation of sodium citrate buffer, citric acid and sodium citrate were added. Citric acid is a weak acid that provides buffering capacity, while sodium citrate is the sodium salt of citric acid, which helps adjust the solution's pH. The addition of powders was carefully monitored to ensure complete transfer and minimize any loss. The specific amounts of powders added were as follows:

Tris Buffer (200 L):

Sodium Citrate Buffer (200 L):

Tris NaCl: 11.69 kg Tris base: 1.212 kg Tris HCl: 0.63 kg Citric Acid: 1.92 kg Sodium Citrate: 9.6 kg

For other volumes, the amounts were scaled proportionally to maintain the same final concentration. This scaling ensures the final buffer solutions have consistent properties, regardless of the volume being prepared.

Mixing Procedure

The mixing process was monitored through two distinct mixing times. Mixing Time 1 was determined by measuring conductivity and pH. Conductivity measures the ionic strength of the solution, indicating the extent of powder dissolution. pH measures the acidity or alkalinity of the solution, which is crucial for buffering capacity. This time was defined as the point when 99% of the final conductivity value was achieved, with subsequent measurements remaining within a 1%

tolerance for at least 5 minutes. Similarly, 95% of the final pH value was reached and maintained within a 5% tolerance for at least 5 minutes. These criteria ensured the solution reached a stable state and that the powders were fully dissolved. Mixing Time 2 was determined by visual inspection, defined as the point when all suspended particles were visibly dissolved. This was verified using external and submersible cameras to inspect the four bottom corners of the bag. The total mixing time was recorded as the longer duration between Mixing Time 1 and Mixing Time 2. This approach ensured the solution was fully homogeneous and no undissolved particles that could affect buffer performance remained. Upon achieving the desired mixing, the Flexsafe® Bags were topped up with deionized water to reach the final volume of 100%. This step ensured the final concentration of the solution was accurate and ready for use. A final visual inspection was conducted to ensure the complete dissolution of the powders. This step was crucial to confirm the homogeneity and readiness of the buffer solutions for subsequent use. Any undissolved particles could affect buffer performance and lead to inconsistent results in downstream applications.

Finally, multiple batches of Tris and sodium citrate buffers were prepared using the same protocol to assess the reproducibility of the mixing process. The results showed consistent mixing times and final buffer properties across different batches, demonstrating the reliability of the Flexsafe® Pro Mixer system. The reproducibility of the results was further confirmed by statistical analysis, which showed low variability in the mixing times and buffer properties.

Analytics

Conductivity and pH Measurements

Conductivity and pH were measured at regular intervals during the mixing process to monitor the dissolution of the powders. The measurements were taken using calibrated instruments to ensure accuracy. The results showed that the conductivity and pH values reached stable levels within the specified mixing times, confirming the complete dissolution of the powders. The stability of the conductivity and pH values over time was also monitored to ensure the buffers remained stable during storage.

Visual Inspection

Visual inspections were conducted using external and submersible cameras to verify the complete dissolution of the powders. The inspections were performed at multiple points in the Flexsafe® Pro Mixer Bags to ensure there were no undissolved particles. The results showed clear and homogeneous solutions, confirming the effectiveness of the mixing process. The visual inspections were supplemented by microscopic analysis, which confirmed the absence of any undissolved particles or aggregates.

Stability Tests

The stability of the prepared buffers was assessed by storing the solutions at different temperatures and monitoring the conductivity and pH over time. The results showed that the buffers remained stable for extended periods, with no significant changes in conductivity or pH. This stability is important for ensuring the reliability and reproducibility of the buffers in downstream applications.

Particle Size Measurements

To capture particle sizes, a digital microscope was connected to a computer running DinoCapture 2.0 software. The sample was placed under the microscope, and the focus was adjusted to obtain clear images of the particles. Calibration was performed using a slide with a known scale to set accurate measurement parameters within the software.

The software's measurement tools were then employed to outline and measure the particles directly on the captured images, as shown in Figure 2, for one sample (Tris), allowing for the determination of dimensions such as diameter and area. Real-time data provided by the software facilitated immediate review and documentation of particle sizes, ensuring precision and efficiency in the measurement process.

CFD Model

We used a Lattice-Boltzmann (LB)-based CFD approach with Lagrangian particle tracking for the computational results, and we compared the results to experimental data. The results of both methods can be seen as a convolution of complex physical phenomena like fluid hydrodynamics, particle motion, a coupling of both, and dissolution mechanics. The LB CFD code M-Star CFD (M-Star Simulations LLC, Version 3.10.32) was used.

A sophisticated CFD model that can accurately reproduce the experimental findings needs to be transient, highly resolved and fast to solve, ideally on desktop resources. We applied an LB code and executed it on GPUs to achieve the required performance for the hydrodynamics and the particle dynamics. Figure 3 demonstrates the digital geometry used for the simulations.

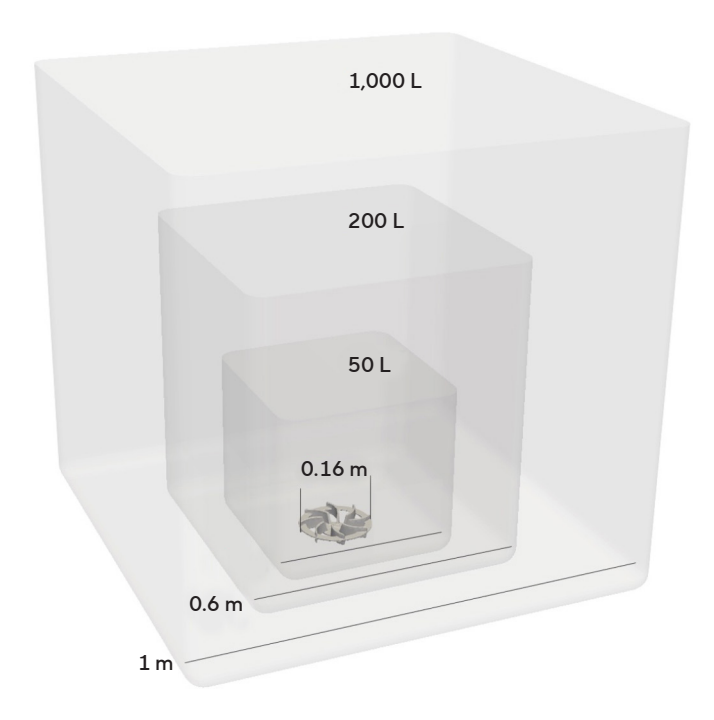
Figure 2: Particle Size Distribution for Components (A) Tris HCl, (B) Tris Base, and (C) Tris NaCl







Figure 3: Computational Domain and Dimensions



Hydrodynamics

The validity of the hydrodynamic flow prediction of Lattice-Boltzmann LES simulations has been shown previously.
We solved the three-dimensional, time-dependent incompressible Navier-Stokes equations for the hydrodynamics:

1.
$$\frac{\partial \vec{u}}{\partial t} + \vec{u} \times \nabla \vec{u} = g - \frac{\nabla p}{\rho} + \nabla \cdot (\nu \nabla \vec{u}) + \frac{F_p}{\rho}$$

Here, \vec{u} is the fluid velocity, g is the acceleration due to gravity, p is the pressure and v is the kinematic viscosity. The forces from the fluid-particle coupling are F_P . This is the sum of all particle forces (drag force, virtual mass, and gravity) over all particles at a given location. The liquid continuous phase is incompressible:

2.
$$\nabla \times \vec{V} = 0$$

We used a Large Eddy Simulation (LES) turbulence model with a Smagorinsky closure term to account for sub-grid turbulent effects.¹² The effective viscosity v is modified such that:

3.
$$v = v_0 + v_1$$

Where v_0 is the molecular viscosity and v_t is the sub-grid eddy viscosity:

4. vt =
$$(C_S \Delta_X)^2 \bar{S}$$

Where C_S = 0.1 is the empirical Smagorinsky coefficient, Δ_X is the lattice spacing and S represents the norm of the filtered strain rate tensor.

The advection-diffusion equation was used for scalar transport. In this case, the scalar represents the dissolved ions, written as:

5.
$$\frac{\partial c}{\partial t} + \nabla \times (\vec{u}c) = \nabla \times (D\nabla c) + \dot{c}$$

Where c denominates the local concentration and D the diffusion coefficient of the substance. A source term \dot{c} is added to implement the concentration change due to particle dissolution. Highly resolved LES turbulence modeling has been shown to accurately predict scalar transport in turbulent stirred systems. ^{6,14}

In addition, we solve the free surface dynamics to check for vortex formation. 15,16,17

A turbulence wall function was also applied to account for near-wall turbulence effects. ¹⁸ The prediction of the dissolution dynamics was not successful without this wall model, as the salt particles would otherwise settle on the bottom wall, where they would be dispersed and dissolved.

Lagrangian Particles

The dissolving particles were tracked with a Lagrangian framework where each particle or parcel had its own individual properties. This method can be used for a variety of particle types, such as bubbles, droplets, or solid particles.¹⁹ Parcels can be used to improve the performance and speed of the simulation.¹⁷ Forces and masses can be scaled by a number scale, which defines how many particles are represented by one parcel. A number scale of 10 was applied to all parcels in all simulations.

The acceleration of a parcel was expressed as:

6.
$$\vec{ma} = \vec{F}_g + \vec{F}_{vm} + \vec{F}_d$$

with ${\bf m}$ as the parcel mass and $\vec{{\bf a}}$ as the acceleration and the major forces: $\vec{{\bf F}}_{\rm g}$ as the force due to gravity | buoyancy, $\vec{{\bf F}}_{\rm vm}$ as the virtual or added mass force, and $\vec{{\bf F}}_{\rm d}$ as the drag force.

The effect of gravity | buoyancy was given as:

7.
$$\vec{F}_q = (\rho_f - \rho_p) V_p \vec{g}$$

with the fluid density $\rho_{\rm F}$ particle density $\rho_{\rm p}$ parcel volume $V_{\rm p}$ and the gravitational acceleration vector $\vec{\bf g}$ with $[0, -9.81, 0]~{\rm m/s^2}$. The virtual or added mass force describes the inertia of the fluid that surrounds the parcel and is transported along with it:

8.
$$\vec{F}_{vm} = \left(2.1 - \frac{0.132}{0.12 + A_c^2}\right) V_p \rho_f \left[\frac{\frac{d}{dt}(\vec{u} - \vec{v})}{2}\right]$$

with:

9.
$$A_c = \frac{(\vec{u} - \vec{v})^2}{d_p \frac{d}{dt} (\vec{u} - \vec{v})}$$

Here, \vec{v} represents the parcel velocity, and d_p is the particle diameter.

The drag force represents the resistance of the fluid medium. It is one of the major forces and was included in all particle simulations:

10.
$$\vec{F}_d = \frac{\pi}{8} C_d d_p^2 \rho_f | \vec{u} - \vec{v}| (\vec{u} - \vec{v})$$

The drag coefficient for spheres was calculated using the drag coefficient \mathbf{C}_{D} as a common, modified Schiller-Naumann correlation.²¹

11.
$$C_D = \frac{24}{Re_p} (1+0.15 Re_p^{0.681}) + \frac{0.407}{1+\frac{8710}{Re_p}}$$

The fluid forces were fully coupled with the particle forces according to Newton's Third Law:

12.
$$\vec{F}_{fj} = -\sum_{1}^{I} (\vec{F}_{g} + \vec{F}_{vn} + \vec{F}_{d})$$

where index j represents the fluid cell or voxel, and the sum includes all parcels indexed with i within this cell. Minor forces like the lift force and the pressure gradient force were neglected in this model.

Dissolution

The dissolution of particles can be described as a mass flow $\dot{\mathbf{m}}_{x}$:

13.
$$\dot{m}_{p} = k_{Lp} A_{p} (S_{c} - c_{f})$$

with a mass transfer coefficient $k_{\text{L,p}}$. The mass flow scales with the particle surface area A_{p} , a solubility S_{c} and the local fluid mass concentration c_{f} . We assumed that the buffer salt particles fully consisted of one species.

The mass transfer coefficient is specified as:

$$14. \quad k_{L,p} = Sh_p \frac{D}{d_p}$$

With the species diffusion coefficient D, the particle diameter d_p , and the Sherwood number Sh_p , which describes the ration of convective to diffusive mass transfer.

15.
$$Sh_p = 2.0 + 0.44 Re_p^{0.5} \left(\frac{V_0}{D}\right)^{0.38}$$

The particle Reynolds number is defined as $Re_p = |\vec{u} - \vec{v}| d_p/v$.

Table 1 lists the critical input parameters and their values.

Table 1: Input Particle Parameters

Input Parameter	Unit	Sodium Citrate	Tris NaCl	Tris HCI	Tris Base
Sauter Mean Diameter d32	m	0.00095	0.00074	0.0013	0.0011
Solubility, Sc	kg/m³	720	380	683.5	561
Diffusion Coefficient, D	m²/s	8.00 × 10 ⁻¹⁰		1.00 × 10 ⁻⁹	
Density, rho_p	kg/m³	1,760	2,170	1,280	1,320

Results

Experimental Results

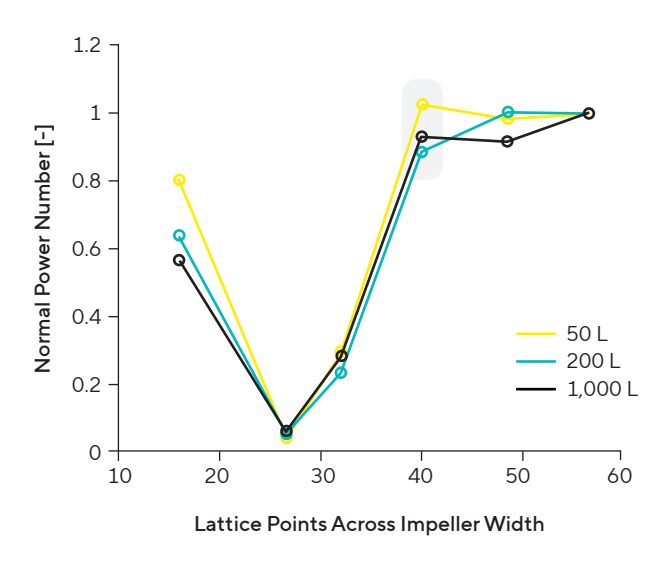
The results demonstrated that the Flexsafe® Pro Mixer system was highly efficient in preparing Tris and sodium citrate buffers across various volumes. For the Tris buffer, the mixing times were less than 5 minutes for all tested volumes (50 L, 200 L, and 1,000 L). Similarly, for sodium citrate buffer, the mixing times were less than 5 minutes for the 50 L and 200 L volumes, and less than 10 minutes for the 1,000 L volume. These results highlight the rapid and consistent performance of the Flexsafe® Pro Mixer system in achieving complete dissolution of powders and uniform buffer preparation. The short mixing times are particularly advantageous in biomanufacturing processes, where time is a critical factor. The ability to prepare large volumes of buffer quickly and efficiently can significantly improve the overall productivity of the manufacturing process.²²

Numerical Results

Grid Convergence and Single-Phase Flow

The numerical grid must be fine enough to resolve all major flow structures. Theoretically, all structures from the Taylor length scale down to the isotropic turbulence region should be resolved. Since it is not possible to estimate the exact dimensions of these scales, we present a grid study based on the normalized power number in Figure 3. A resolution of 40 cells across the impeller is sufficient to make the total power input sufficiently grid-independent.

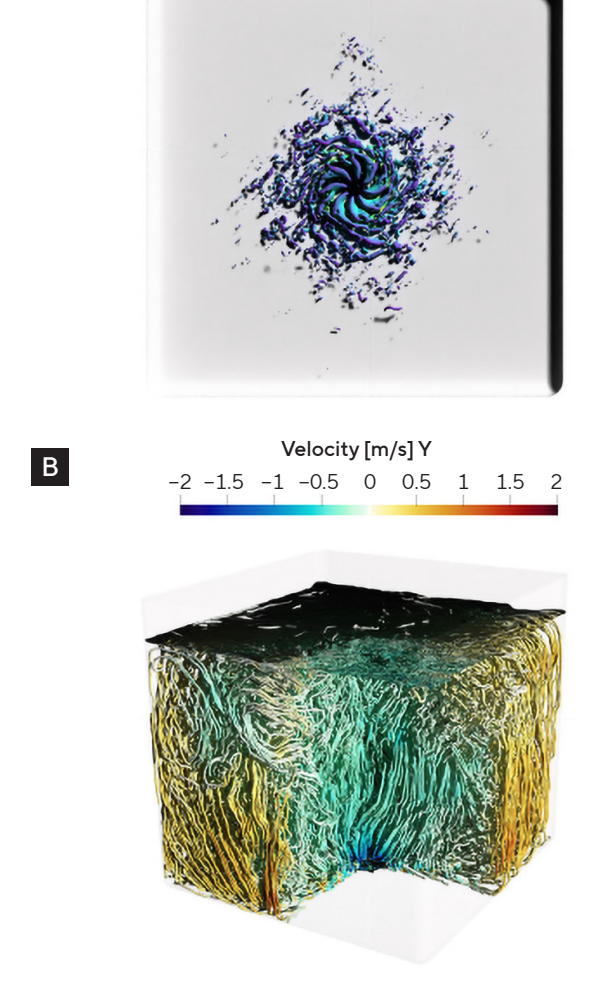
Figure 3: Grid Study of All Geometries. The Chosen Resolution is Highlighted as a Grey Box.



The instantaneous flow structure reveals the expected rotating trailing vortices, as shown in Figure 4. The Q-criterion colored by velocity magnitude is used to show the topology of these vortices. The topology of the streamlines suggests a strong axial component of the flow in the bulk. The rectangular shape of the vessel disrupts the rotation of the flow and directs it upward near the side walls, causing a similar effect to baffles in a classical circular reactor. Consequently, the fluid flows downward at the center of the vessel, where it is accelerated by the impeller and moves toward the side walls along the bottom wall. This produced fast mixing and drives the salt particles towards the impeller, where we observed the highest velocities and fast dissolution as a result.

Figure 4: Rendered Q-Criterion **(A)** Colored by Velocity Magnitude And Streamlines **(B)** Colored by The Axial Velocity Component.

Velocity Magnitude [m/s]



Note. The image shows the instantaneous flow of the 1,000 L vessel at 750 rpm.

All experimental and numerical dissolution studies are compared in Figure 5. This includes the three different scales for two different solid substances. The addition happens during the phase indicated by the grey boxes. This means that each physical and numerical experiment has two phases: an initial phase, during which the salt particles are added above the air-water interface, and the second phase, when all particles have entered the system and dissolved completely. The dissolution of the particles starts as soon as they enter the liquid phase.

We acknowledge that some details of the addition might differ between the simulation and experimental measurements. We assume a constant addition rate for the first phase. The slower start in the experiments might result from that assumption, or from physical effects not considered, like a delay due to wetting of the particles. However, the overall agreement is very good considering that the model only requires process parameters, material properties, and initial particle size distributions as input. No fitting parameters or calibrations are necessary. Overall, the Tris salt dissolves faster than sodium citrate, mainly due to its smaller initial particle size.

The total ion flux is shown in Figure 7. We integrated the ion flux over time for each voxel. The time-averaged particle residence time shows a very similar topology (data now shown).

Figure 5 Comparison of Experiments and Simulations. The Concentrations are Normalized. The Addition Phase is Indicated by Grey Boxes. Multiple Experiments are Shown, When Available

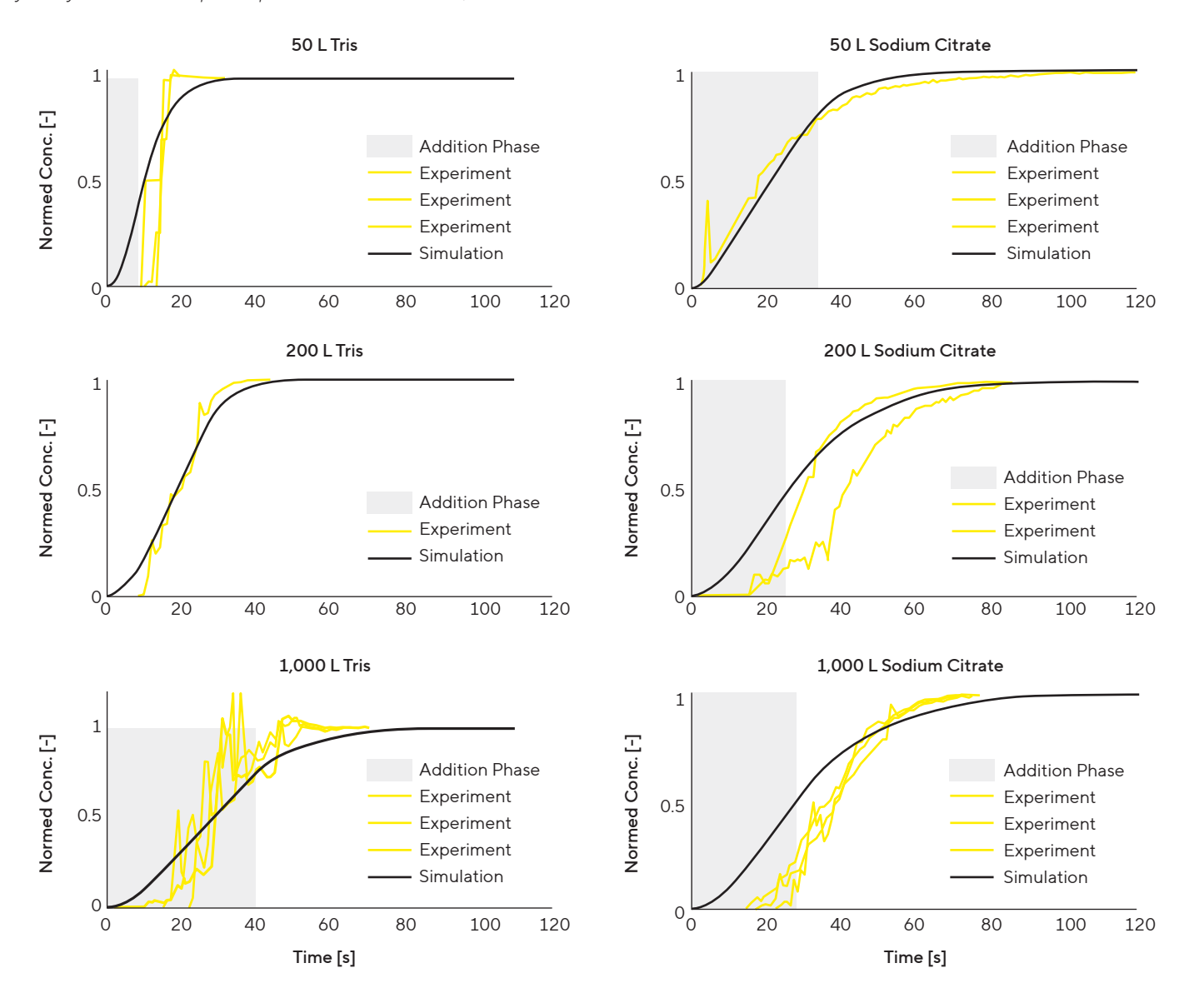
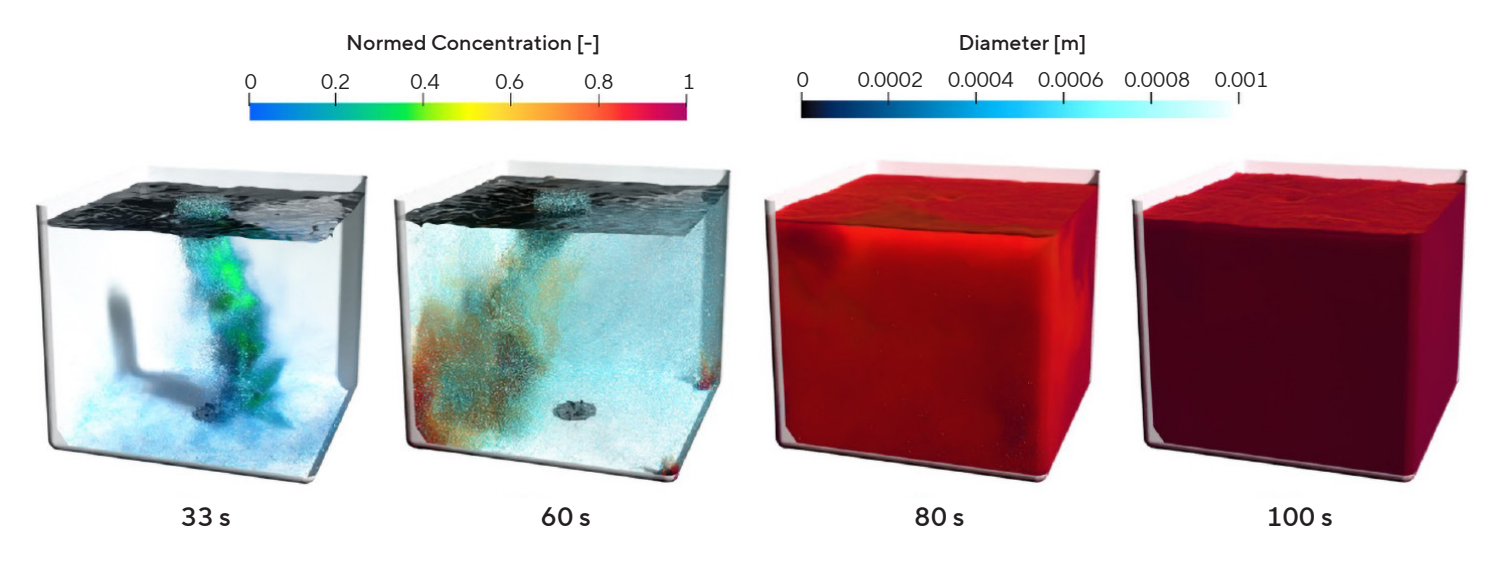


Figure 6 Dissolution Process at Different Time Points. The Particles are Colored by the Diameter, and the Volumetric Concentration is Normalized



Note. Each Lagrangian parcel represents 10 particles. The particle diameter is scaled by three to enhance visibility.

The regions of highest total ion flux are the corners, where small particles with high specific surface areas fully dissolve. There is also a region of high ion flux near the impeller and below the addition region. The design is very simple, as no baffles or similar structures are required to enable efficient dissolution, making it suitable for single-use applications.

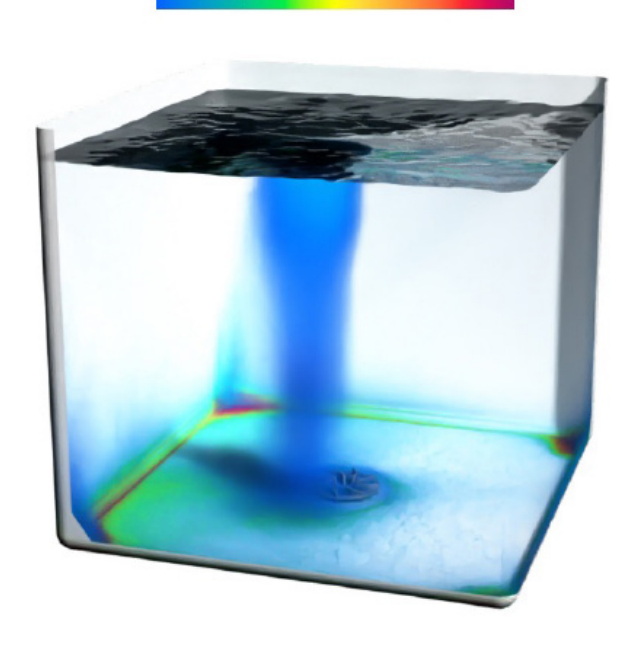
Figure 7 Total Ion Flux as Volumetric Rendering Locally Integrated Over Time

Total Ion Flux [Mol]

0.003

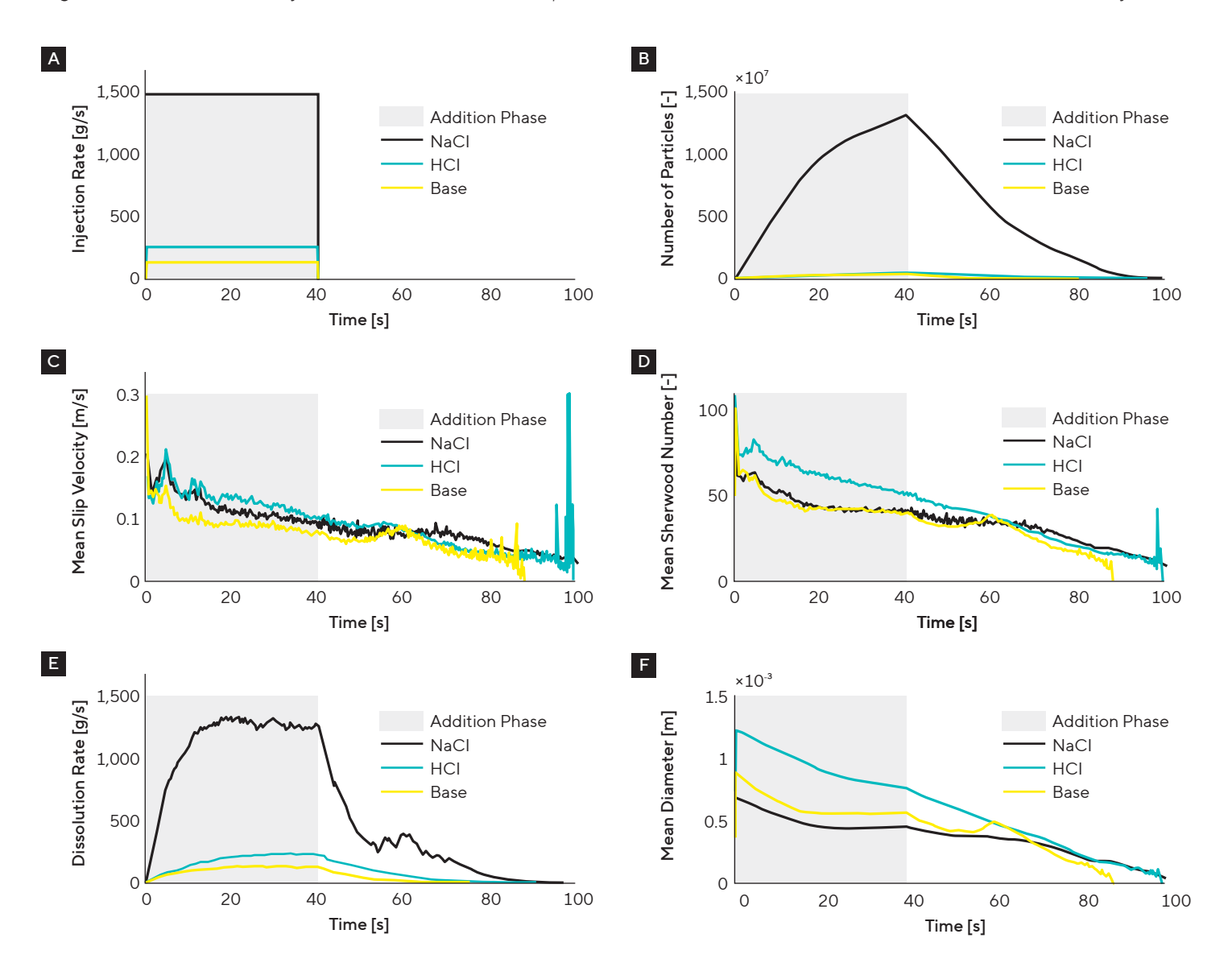
0.004

0.002



Various particle and dissolution-related graphs of the CFD simulation of the 1,000 L Tris buffer case are shown in 8. The injection rate is shown in Figure 8A. We assumed a constant addition rate for 40 seconds. The number of particles is shown in Figure 8B. We observed a constant increase in the particle number until about 20 seconds, when some of the smaller added particles started to fully dissolve. The amount decreases after the addition. The mean slip velocity is shown in Figure 8 C. It starts at values around 0.1-0.2 m/s and becomes smaller as the particles become smaller and the forces shift from being mostly driven by gravity to being more driven by drag forces. Consequently, the Sherwood number (Figure 8D), which is the driving mechanism for the dissolution, follows that trend. The total dissolution rate plateaus after around 20 seconds and remains constant until the addition is finished. Then, fewer particles lead to lower dissolution rates. The mean particle diameter decreases from start to finish (Figure 8E) as expected.

Figure 8 Various Particle Dynamics For The Three Components of the Tris Buffer Over Time for the 1,000 L Geometry



Conclusion

The Flexsafe® Pro Mixer system demonstrated exceptional efficiency and reliability in the preparation of Tris and sodium citrate buffers. The methodology outlined in this study provides a robust framework for buffer preparation in biomanufacturing applications. The rapid mixing times and consistent results across different volumes demonstrate the system's capability to meet the demands of large-scale buffer preparation, ensuring high-quality and reproducible outcomes.

This study contributes valuable insights into the optimization of buffer preparation processes, supporting the advancement of biomanufacturing technologies. The findings are consistent with previous research on the performance of single-use mixing systems, which have been shown to offer significant advantages in terms of flexibility, scalability, and ease of use. 10,12 The use of single-use systems can also reduce the risk of cross-contamination and lower the overall cost of buffer preparation, making them an attractive option for biomanufacturing applications. ⁴ The CFD simulations showed good agreement with the measured data without relying on any fitting parameters, suggesting that the underlying mechanics work effectively. This agreement allows CFD simulations to be a robust tool to reduce the number of experiments and wet runs, accelerating the manufacturing of biopharmaceuticals.

References

- Lakatos, D., Idler, M., Stibitzky, S., Amann, J., Schuschkewitz, J., Krayl, D., et al. (2024). Buffer system improves the removal of host cell protein impurities in monoclonal antibody purification. Biotechnology and Bioengineering, 3869-3880.
- Ram, N., Johnson, J., Ardeshna, H., Camire, J., Campbell, R., Chau, D., & Gardner, S. (2023). Evaluation of the design, development, and performance of a mass-flow based, open-source buffer manufacturing system. PDA Journal of Pharmaceutical Science and Technology, 79-98.
- 3. Carredano, E. N., Westin, S., Busson, K., Karlsson, T. M., Blank, T. S., et al. (2018). Simplification of buffer formulation and improvement of buffer control with in-line conditioning (IC). Biopharmaceutical Processing, 513-525.
- 4. Satzer, P. (2024). A risk-aware assessment for buffer recycling across unit operations for monoclonal antibody purification and its potential. Biochemical Engineering Journal.
- Seidel, S., Schirmer, C., Maschke, R., Rossi, L., Eibl-Schindler, R., & Eibl, D. (2023). Computational fluid dynamics for advanced characterization of bioreactors used in the biopharmaceutical industry: part I: literature review. Computational Fluid Dynamics-Recent Advances, New Perspectives and Applications, 53-82.
- Fitschen, J., Hofmann, S., Wutz, J., Kameke, A. V., Hoffmann, M., Wucherpfennig, T., & Schlüter, M. (2021). Novel evaluation method to determine the local mixing time distribution in stirred tank reactors. Chemical Engineering Science: X, 10.
- 7. Hagel, L., Jagschies, G., & Sofer, G. (2007). Handbook of process chromatography: Development, manufacturing, validation and economics. In Handbook of Process Chromatography: Development, Manufacturing, Validation and Economics.
- 8. Eibl, R., Kaiser, S., Lombriser, R., & Eibl, D. (2010). Disposable bioreactors: the current state-of-the-art and recommended applications in biotechnology. Applied Microbiology and Biotechnology, 86(1), 41–49.
- 9. Shukla, A. A., & Gottschalk, U. (2013). Single-use disposable technologies for biopharmaceutical manufacturing. Trends in Biotechnology, 31(3), 147–154.
- 10. Hofmann, S., Weiland, C., Fitschen, J., von Kameke, A., Hoffmann, M., & Schlüter, M. (2022). Lagrangian sensors in a stirred tank reactor: Comparing trajectories from 4D-Particle Tracking Velocimetry and Lattice-Boltzmann simulations. Chemical Engineering Journal, 449.
- 11. Kuschel, M., Fitschen, J., Hoffmann, M., von Kameke, A., Schlüter, M., & Wucherpfennig, T. (2021). Validation of novel Lattice Boltzmann large eddy simulations (LB LES) for equipment characterization in biopharma. Processes, 9(6).

- 12. Yu, H., Girimaji, S. S., & Luo, L. S. (2005). DNS and LES of decaying isotropic turbulence with and without frame rotation using lattice Boltzmann method. Journal of Computational Physics, 209(2), 599–616.
- 13. M-Star Simulations LLC. (2024, September 18). https://docs.mstarcfd.com/17_Theory/large-eddy-simulation-review.html.
- 14.J. Thomas, et al. (2021). Predicting gas-liquid mass transfer rates in reactors using a bubble parcel model. Chemical Engineering Science, 264.
- 15. Farsani, H. Y., Wutz, J., DeVincentis, B., Thomas, J. A., & Motevalian, S. P. (2022). Modeling mass transfer in stirred microbioreactors. Chemical Engineering Science, 248.
- 16. Schlaich, E. M., Thomas, J. A., Kandari, L., Tremml, G., & Khetan, A. (2023). Experimental and computational characterization of mass transfer in high turndown bioreactors. Biotechnology Progress, 39(3).
- 17.J. A. Thomas, et al. (2023). Modeling free surface gas transfer in agitated lab-scale bioreactors. Chemical Engineering Communications, 210(8), 1328–1339.
- 18. Cai, S. G., & Sagaut, P. (2021). Explicit wall models for large eddy simulation. Physics of Fluids, 33(4).
- 19. Sirasitthichoke, C., Teoman, B., Thomas, J., & Armenante, P. M. (2022). Computational prediction of the just-suspended speed, Njs, in stirred vessels using the lattice Boltzmann method (LBM) coupled with a novel mathematical approach. Chemical Engineering Science, 251.

- 20. J. A. Thomas, et al. (2022). A CFD Digital Twin to Understand Miscible Fluid Blending. AAPS PharmSciTech, 22(3).
- 21. Michaelides, E. E., Sommerfeld, M., & van Wachem, B. (2022). Multiphase Flows with Droplets and Particles, Third Edition. CRC Press.
- 22. Langer, E. S., & Rader, R. A. (2014). Single-use technologies in biopharmaceutical manufacturing: A 10-year review of trends and the future. Engineering in Life Sciences, 14(3), 238–243.

Germany

Sartorius Stedim Biotech GmbH August-Spindler-Strasse 11 37079 Goettingen Phone +49 551 308 0

For more information, visit sartorius.com

USA

Sartorius Stedim North America Inc. 565 Johnson Avenue Bohemia, NY 11716 Toll-Free +1 800 368 7178